



Short Communication

Macroscopically uniform and flat lithium thin film formed by electrodeposition using multicomponent additives

Kazuhiro Fukami^{a,*}, Akihiro Sakurai^a, Takamitsu Tsujimoto^b, Masaki Yamagami^a,
 Atsushi Kitada^a, Kota Morimoto^c, Kiho Nishioka^c, Shuji Nakanishi^c, Yusuke Yoshikane^b,
 Toshimitsu Nagao^b, Jun-ichi Katayama^b, Kuniaki Murase^a

^a Department of Materials Science and Engineering, Kyoto University, Kyoto 606-8501, Japan

^b Okuno Chemical Industries Co. Ltd., Osaka 538-0044, Japan

^c Research Center for Solar Energy Chemistry, Graduate School of Engineering Science, Osaka University, Osaka 560-8531, Japan



ARTICLE INFO

Keywords:

Lithium
 Electrodeposition
 Additive
 Multicomponent
 Dendrite-free

ABSTRACT

It is well-known that the electrodeposition of lithium usually results in the formation of dendrites on the electrode surface. This limits the utilization of metallic lithium as a material for, for example, the negative electrodes of rechargeable batteries. In aqueous solutions, similar dendritic growth of metals is often observed during electrodeposition; however, utilization of multicomponent additives has overcome this shortcoming. Here, we report that the simultaneous utilization of four different additives greatly suppresses the formation of lithium dendrites during electrodeposition in a tetraglyme-based solution. The roles of the additives are discussed, based on the results of electrochemical quartz crystal microbalance measurements and X-ray photoelectron spectroscopy.

1. Introduction

Metallic lithium is regarded as a promising negative electrode material for next-generation rechargeable batteries. Currently, thin films of lithium metal used in the assembly of such batteries are produced mainly by flat rolling processes in an Ar-filled atmosphere. Since the roughness of the lithium surface directly affects the initiation of dendritic growth during the subsequent charging of batteries, it is of great importance to prepare a macroscopically flat and smooth lithium surface, free from unevenness like dendrites [1–10]. Electrodeposition has been considered as a promising technique to obtain lithium thin films at a low cost, as in the case of electrolytic copper foil. However, it is widely accepted that dendritic growth is inevitable during the electrodeposition of lithium without additives [1]. Such dendritic growth is a fatal issue not only for the subsequent charging of batteries but also for the mass production of lithium thin films by electrodeposition.

Dendritic growth during electrodeposition was also a serious issue in the electrodeposition of metals in aqueous solutions. This problem was overcome step by step by the development of additives. In electrodeposition from aqueous baths, different types of additives such as levelers and brighteners are generally used to obtain macroscopically flat and

smooth metal surfaces [11]. On the other hand, considering the electrodeposition of lithium, the number of additives developed so far is much fewer than those developed for use in metal electrodeposition using aqueous baths [12–14]. Furthermore, the number of studies on the electrodeposition of lithium using multicomponent additives is still limited [15,16], although electrodeposition in aqueous solutions mostly involves multicomponent additives. Therefore, it is of great importance to study possible additives for lithium deposition and to test their combinations, as well as to understand their mechanisms.

In the present study, we report four newly found additives effective for the electrodeposition of a macroscopically flat lithium thin film when they are used simultaneously. The roles of the additives are studied by electrochemical quartz crystal microbalance (EQCM) measurements and X-ray photoelectron spectroscopy (XPS).

2. Experimental

All the experiments were carried out in an Ar-filled glove box (GBJV080, GloveBox Japan Inc.) with O₂ content below 5 ppm and with a dew point below –75 °C. Tetraethyleneglycol dimethyl ether (Acros Organics, 99%) was used as the solvent and will be denoted as G4 in this

* Corresponding author.

E-mail address: fukami.kazuhiro.2u@kyoto-u.ac.jp (K. Fukami).

<https://doi.org/10.1016/j.elecom.2022.107238>

Received 13 January 2022; Received in revised form 28 January 2022; Accepted 1 February 2022

Available online 4 February 2022

1388-2481/© 2022 The Author(s). Published by Elsevier B.V. This is an open access article under the CC BY license (<http://creativecommons.org/licenses/by/4.0/>).

paper. Before utilization, the residual water in G4 was removed with molecular sieve 3A (Nacalai Tesque Co. Ltd.) over 24 h. Note that the residual water in the solutions is not considered as an additive in the present study. Lithium bis[(trifluoromethyl)sulfonyl]imide (denoted as LiTf₂N) was used as the lithium precursor. A solution with a molar ratio of G4:LiTf₂N = 4:1 was prepared and used as the bath without additives.

As additives, 2-butyne-1,4-diol (BASF Japan, 95.0%), 2-naphthol (Tokyo Chemical Industry, 99.0%), saccharin (FUJIFILM Wako Pure Chemical Corporation, 98.0%), and diacetone acrylamide (Nihon Kasei, 98.0%) were used at concentrations of 0.2 g L⁻¹, 1 g L⁻¹, 1 g L⁻¹, and 1 g L⁻¹, respectively. Before adding the additives to G4, they were dried under vacuum conditions at 60 °C for 24 h followed by drying at 80 °C

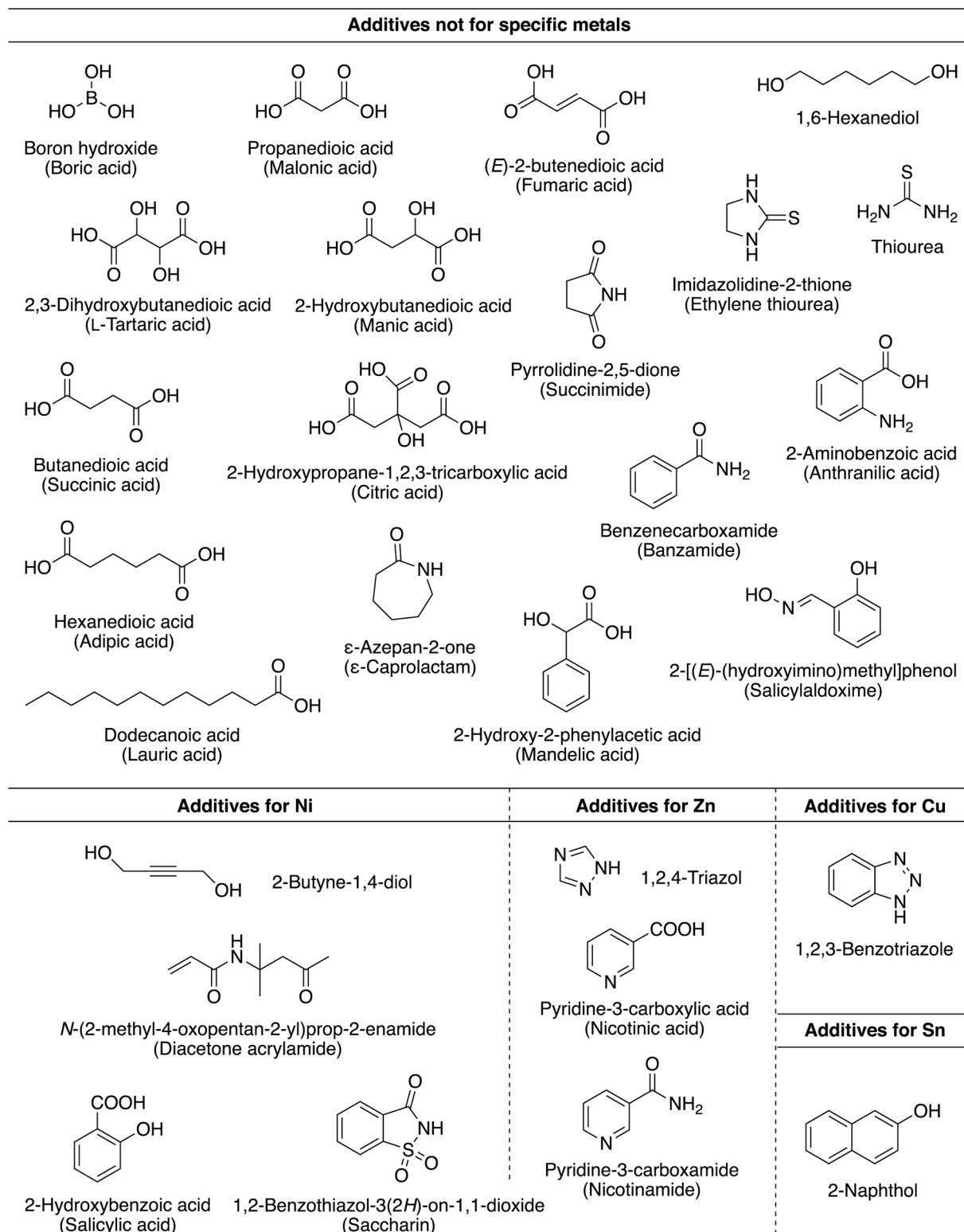


Fig. 1. Twenty-seven additives evaluated in the present study. The additives are categorized according to their conventional uses in aqueous solutions (additives not for specific metals, for Ni, for Zn, for Cu, and for Sn electrodeposition).

for 24 h. A nickel (Ni) sheet 10 mm × 50 mm in size was used as the working electrode (10 mm × ~20 mm was dipped into the solution). The Ni sheet was polished with 0.3 μm alumina powder before use. For the EQCM measurements, Ni on a quartz electrode with a diameter of 10 mm (EC Frontier, QA-A9M) was employed. All the electrochemical measurements were carried out using a three-electrode cell with a potentiogalvanostat (Biologic Science Instruments, SP-150) and a QCM system (Seiko EG& G, QCA922). Lithium sheets (purity 99.8%, Honjo Metal) were used as the counter and reference electrodes. The chemical states of sample surfaces were characterized by XPS (JEOL, JPS-9010TRX with Mg-Kα) with 10 kV and 20 mA of emission current. Ar⁺ etching was performed at an acceleration voltage of 1 kV. Calibration of XPS data was carried out using a hydrocarbon peak in C 1 s at 285.0 eV.

3. Results and discussion

Screening of additives known for electrodeposition in aqueous baths. Our strategy to find effective additives for lithium deposition is to screen well-known additives used in aqueous baths. Since the number of additives used for aqueous electrodeposition is huge, there are a number of know-how and experience to select the additives for an electrodeposition system of interest. With this approach, one can save time until effective multicomponent additives and their combinations are found. Fig. 1 summarizes the chemicals which we evaluated for macroscopically flat lithium deposition. It should be noted that we originally chose more chemicals than those shown in Fig. 1; however, most of them were insoluble in G4. Thus, we chose the chemicals in Fig. 1 (all of which dissolved in G4) for further evaluation. As shown in Fig. 2(a), the electrodeposition of lithium takes place non-uniformly in an additive-free bath. Note that the applied potential (−1.0 V vs. Li⁺/Li) was selected so that a large cathodic current density was detected at the potential in the cyclic voltammogram and the morphology after lithium deposition

was highly non-uniform with dendritic deposition under the constant potential. Fig. 2(b–e) show typical samples deposited using a single component additive whose surfaces after electrodeposition are relatively good. When 2-butyne-1,4-diol is added to the bath (Fig. 2b), a gray-colored, relatively uniform film is obtained. The central part of the substrate is covered almost uniformly; however, there are mossy aggregates at the edge of the substrate. When saccharin is used as an additive (Fig. 2c), the number of mossy aggregates increases compared with the case of 2-butyne-1,4-diol. On the other hand, one can see a flat surface with a grey-blue color on the flat area after deposition. 2-naphthol is also a good candidate as an additive (Fig. 2d). In this case, the number of mossy deposits decreases, and the surface shows a pale blue color. Diacetone acrylamide results in a different type of deposit (Fig. 2e). The nickel substrate is totally covered with lithium, but the surface appears gray-brown with a non-uniform distribution. It should be noted that lithium films deposited without using any additives were mechanically fragile. The mossy deposit tends to be detached from the substrate during cleaning and drying. Using a single component additive, the lithium deposited on the surface was still fragile; therefore, the differences in the macroscopic morphology of the deposited lithium are hard to find when the surface is cleaned and dried.

Although we tried twenty-seven chemicals including the above four as an additive, none worked as a single component. In addition to experiments with a single component additive, we carried out experiments with different combinations of additives. As clearly observed in Fig. 2f, the film deposited with the simultaneous use of the four selected additives shows a macroscopically flat surface without the formation of mossy aggregates. This result suggests that the use of multicomponent additives is effective for the electrodeposition of lithium.

Roles of the additives evaluated by EQCM. The behavior of lithium deposition and dissolution in a bath containing the four additives was examined. QCM measurements were used and the results were compared with the corresponding electrochemical responses. It is well known that the change in frequency is directly linked to a mass change in accordance with the Sauerbrey equation (Eq. (1)):

$$\Delta f_m = -\frac{2f_0^2}{A\sqrt{\rho_q\mu_q}}\Delta m \quad (1)$$

where Δf_m is the frequency change, f_0 is the reference frequency, A is the electrode area, ρ_q and μ_q are the density and elastic coefficient of the quartz crystal, respectively, and Δm is the mass change. Since the following relation (Eq. (2)) is expected, Δf_m is obtained from the experimental data Δf by subtracting the contribution of $\Delta f_{\eta p}$ that is estimated from the simultaneous measurement of the resonant resistance

$$\Delta f = \Delta f_m + \Delta f_{\eta p} \quad (2)$$

The QCM data were corrected in accordance with the method reported by Serizawa et al., and Δf_m is used in the following discussion [17]. Since lithium is the most light-weight metal, such a correction is essential to estimate Δm from Δf data.

In the present study, cyclic voltammograms were recorded together with QCM measurements. To compare the cyclic voltammograms and QCM responses simultaneously, we calculated the rate of mass change (v_w) and plotted the data against the potential as in the left-hand column of Fig. 3 (a1–e1), denoted as v_w -E hereafter. Note that the vertical axis is inversely determined for ease of comparison with the corresponding cyclic voltammograms. The simultaneously recorded cyclic voltammogram was plotted as in the middle column of Fig. 3 (a2–e2), so that the vertical axis was converted from the current density to the v_w -axis. When the data was converted from current density to v_w , the current efficiency for lithium deposition (Li⁺ + e = Li) and dissolution was regarded as unity (i.e., 100%).

Based on the comparison between the cyclic voltammograms and QCM data, we analysed the role of each additive. To utilize the results of

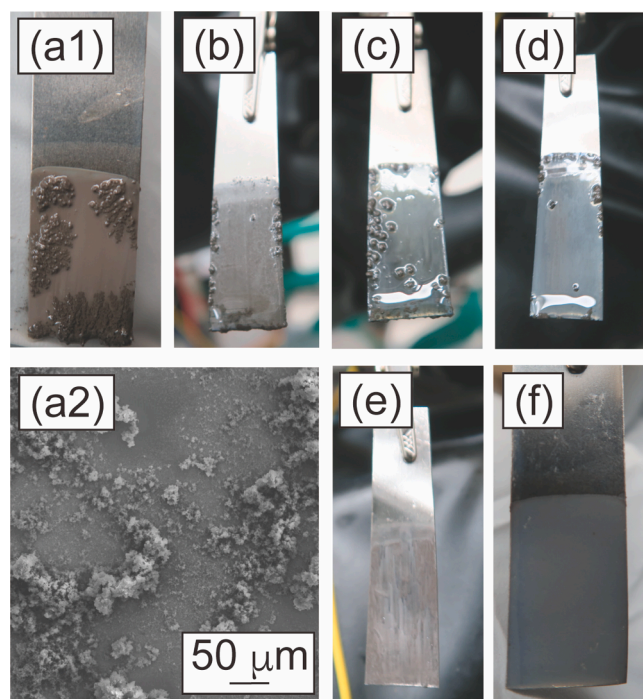


Fig. 2. Photographs of the working electrodes after lithium electrodeposition taken in the glove box. The images (a1), (b), (c), (d), (e), and (f) respectively show the samples deposited without additives, with 2-butyne-1,4-diol, with saccharin, with 2-naphthol, with diacetone acrylamide, and with the four additives. The width of the working electrode was 10 mm. In the case without additives, an SEM image of the surface of lithium is shown in (a2). Electrodeposition was carried out at a constant potential of −1.0 V vs. Li⁺/Li for 5 min.

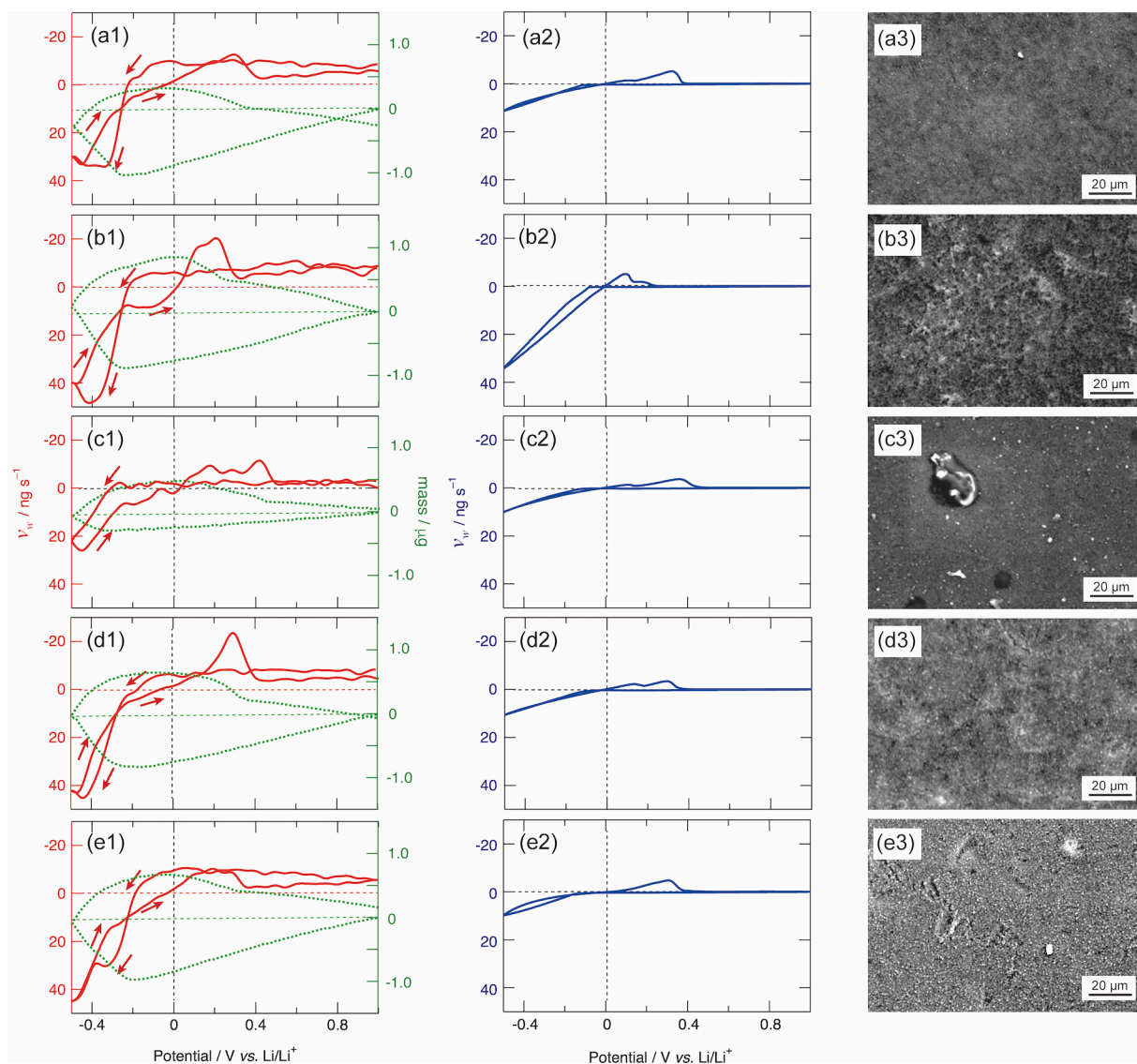


Fig. 3. Cyclic plots of ν_w vs. potential. Plots marked in red in column (1) were measured by QCM, while those in column (2) were measured with the potentiostat. The QCM data were acquired simultaneously with the cyclic voltammograms. The green dotted plots in (1) are the integral of mass rate. The integral of the mass rate at 1.0 V vs. Li⁺/Li before the negative scan is set at zero. The deposition baths in (a) contained all the four additives, in (b) the three additives without 2-butyne-1,4-diol, in (c) without 2-naphthol, in (d) without saccharin, and in (e) without diacetone acrylamide. The scan rate was 10 mV s⁻¹. Typical SEM images of the lithium surface obtained with the four additives and with three additives are shown in column (3). The samples were not exposed to the air before observation. (For interpretation of the references to color in this figure legend, the reader is referred to the web version of this article.)

QCM for comparison with the corresponding cyclic voltammograms, it is important to make the surface of the deposit as smooth as possible to determine $\Delta f_{\eta p}$ as precisely as possible. In the additive-free bath, however, the suppression of dendritic growth is impossible; therefore, we studied the roles of the additives by removing one of the four additives from the bath, which makes it possible to obtain a relatively smooth surface, as observed in the right-hand columns of Fig. 3 (a3–e3), allowing the determination of $\Delta f_{\eta p}$ with relatively good accuracy.

First, the multicomponent bath without 2-butyne-1,4-diol is evaluated as shown in Fig. 3(b). The cathodic behavior is different from the bath with four additives (compare Fig. 3(b2) with Fig. 3(a2)). Without 2-butyne-1,4-diol, the cathodic current density measured electrochemically shows a significant linear increase. This means that without 2-butyne-1,4-diol, intense faradaic decomposition of the electrolyte, the solvent, the three additives, and/or Tf₂N⁻ anions takes place, or the electrodeposition of lithium is promoted for some reason. Since the initiation of so-called dead lithium is unlikely in the case of macroscopically flat deposition and the charge in the lithium stripping under

subsequent anodic polarization is not significantly different between case with the four additives (0.30 μg calculated in the anodic wave) and without 2-butyne-1,4-diol (0.34 μg calculated in the anodic wave), the increase in the current density during the cathodic polarization is mainly due to the decomposition of the solvent, additives, or Tf₂N⁻ which results in the formation of a solid electrolyte interphase (SEI) layer. Indeed, the QCM response reaches a higher ν_w value than with the four additives at ~ -0.4 V. This is due to the formation of a SEI layer on the surface through decomposition. Based on these data, 2-butyne-1,4-diol is expected to adsorb physically on the surface and suppress the electron transfer processes, playing a role as a leveler [18].

The role of 2-naphthol is evaluated by removing it from the bath with the four additives. As shown in Fig. 3(c1), the cathodic response of ν_w obtained by QCM starts to increase at a potential of -0.35 V. In addition, the gradient of the increase in ν_w is gentle compared with the case of the four additives (compare (c1) with (a1)). On the other hand, the electrochemical responses without 2-naphthol and with the four additives are quite similar (compare (c2) with (a2)). This behavior suggests that 2-

naphthol promotes the formation of the SEI to give a steep QCM curve under cathodic polarization.

The QCM and electrochemical behavior without saccharin are shown in Fig. 3(d). Despite the pretty similar electrochemical responses of the bath without saccharin (d2) and with the four additives (a2), the corresponding QCM curves are totally different from each other (compare (d1) with (a1)). Without saccharin, the v_w - E curve measured by QCM gives a clear peak at +0.3 V. This result means that the SEI formed during cathodic polarization is subject to dissolution during the anodic polarization. Therefore, the chemical stability of the SEI formed without saccharin is not high enough and the SEI produced without saccharin is expected to form but dissolve dynamically. Although the clear mechanism of SEI dissolution is not clear, a possible explanation based on XPS results can be found in the last part of this paper.

Finally, the electrochemical behavior without diacetone acrylamide is investigated. When one compares the results in Fig. 3(e) (without diacetone acrylamide) and Fig. 3(a) (with the four additives), the cyclic data look similar to each other, except that a further increase in v_w is detected by QCM at potentials below -0.4 V (Fig. 3(e1)). This behavior suggests that relatively stable chemicals, which are not decomposed on the SEI at a low cathodic overpotential (such as G4 and TF_2N^-), are subject to intense decomposition below -0.4 V without diacetone acrylamide.

Based on the results given above, the main roles of the four additives are assumed to be as follows: (1) 2-butyne-1,4-diol adsorbs on the surface and plays a role as a leveler; (2) 2-naphthol is cathodically decomposed to induce the formation of the SEI; (3) saccharin enhances the stability of the SEI; (4) diacetone acrylamide prevents the cathodic decomposition of G4 and/or TF_2N^- .

SEI characterization by XPS. The chemical states of the SEI formed during electrodeposition with the four additives are characterized by XPS. Fig. 4 shows Li 1 s, O 1 s, C 1 s, F 1 s, N 1 s, and S 2p spectra of the sample. Note that samples for XPS were transferred from the Ar-filled glove box to XPS using a transfer vessel without exposure to the air. From Li 1 s, LiTF_2N (56.5 eV) and LiOH (55.5 eV) are detected before etching. After 2 nm etching, LiTF_2N totally disappears, and LiOH and Li_2O (53.7 eV) become the main components. After 40 nm etching,

metallic lithium is detected together with both a decrease in LiOH and an increase in Li_2O . It should be noted that Li_2O was detected when a commercially available metallic lithium foil was characterized by our XPS apparatus. Thus, the increase in Li_2O may originate from the increase in the content of metallic lithium in the deposited film. From the O 1 s spectrum, LiTF_2N (533.0 eV), Li_2CO_3 (532.3 eV), and LiOH (531.3 eV) are the main components at the surface. After 2 nm etching, LiTF_2N totally disappears as in Li 1 s, and the contribution of Li_2O starts to increase. From C 1 s, the disappearance of LiTF_2N (293.0 eV) after etching is confirmed as well. $(\text{CH}_2\text{OCO}_2\text{Li})_2$ is detected at 286.7 eV at the surface without etching and the intensity becomes almost zero after etching; therefore $(\text{CH}_2\text{OCO}_2\text{Li})_2$ is less likely to be the major component of the SEI. Li_2CO_3 (290.0 eV) starts to contribute after 2 nm etching, suggesting that it is one of the components of the SEI. Looking at the spectrum of F 1 s, coverage of the surface with LiTF_2N (688.9 eV) is confirmed. After 2 nm etching, LiF (685.2 eV) is clearly detected. In the S 2p spectrum, LiTF_2N (169.4 eV) is indeed detected at the surface. Li_2S is detected after 2 nm etching, together with a weak contribution from lithium polysulfide Li_2S_x (166 eV). Note that the photoionization cross section of Li 1 s is two orders of magnitude smaller than those of O 1 s, F 1 s, and S 2p [19]. Therefore, it is quite difficult to clearly detect LiF, Li_2CO_3 and Li_2S_x in the Li 1 s spectrum, given the accuracy of our XPS apparatus. Based on these results, the SEI is expected to be a mixture of Li_2CO_3 , Li_2O , LiF, Li_2S , and Li_2S_x .

The S 2p spectra give more information on the structure of the SEI. At the surface without etching, a non-negligible contribution of Li_2S_x is detected together with the main peak of LiTF_2N . After 2 nm etching, the main contribution changes from LiTF_2N to Li_2S_x . A similar trend is also detected for LiF. On the other hand, Li_2CO_3 and Li_2S are not detectable at the surface, while they start to contribute after 2 nm etching. These results suggest that Li_2S_x and LiF tend to cover the inner SEI of Li_2CO_3 and Li_2S . It has been reported that Li_2S_x compounds are unstable and tend to dissolve in organic solutions [20,21], while Li_2S is stable against dissolution. The origin of the S content is TF_2N^- and/or saccharin. The dissolution of the SEI without saccharin in Fig. 3(d1) is likely due to the formation of Li_2S_x ; therefore, the role of saccharin is presumed to be that it helps the effective formation of Li_2S , while a non-negligible amount of

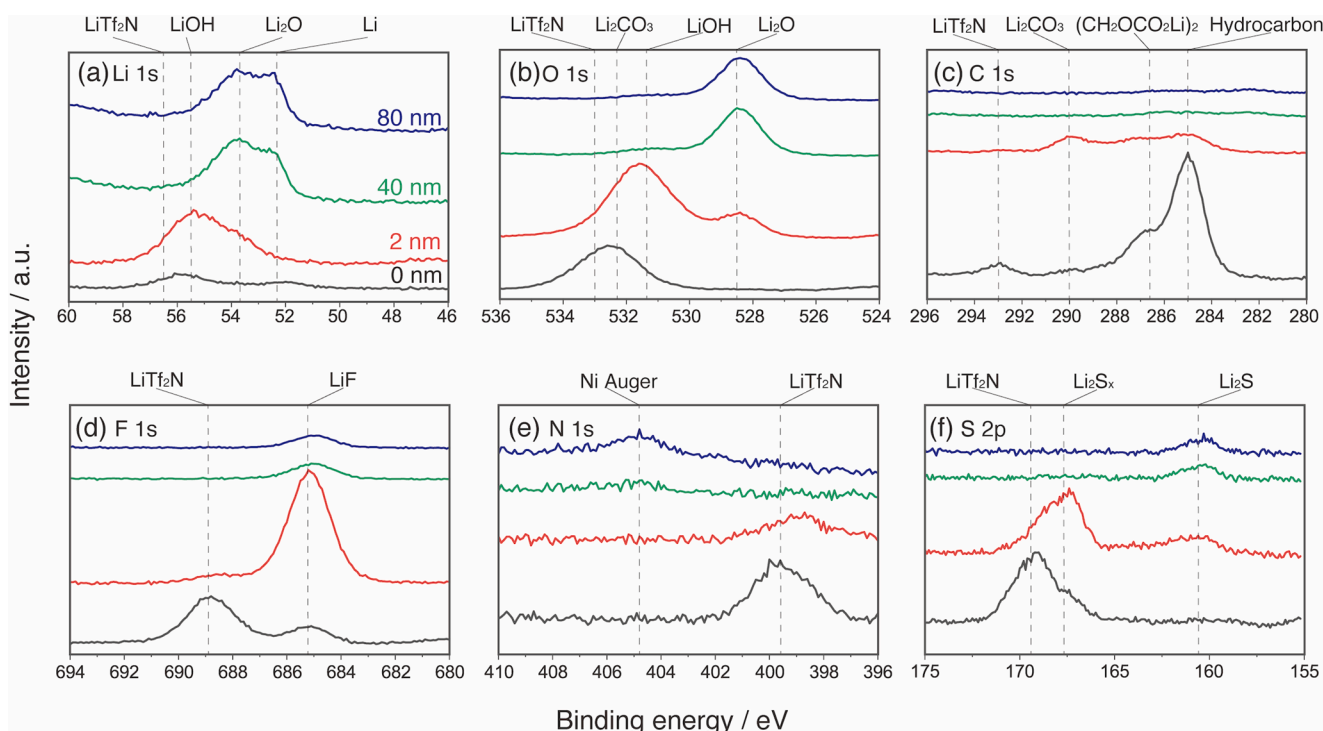


Fig. 4. XPS spectra of a sample prepared by electrodeposition in a bath with the four additives. (a)–(f) Spectra of Li 1 s, O 1 s, C 1 s, F 1 s, N 1 s, and S 2p, respectively.

Li_2S_x may be formed by the decomposition of Tf_2N^- .

Finally, the use of the four additives in the cycle test should be mentioned. For our primitive evaluation, a Li/Li symmetric cell was used. One of the two electrodes was a lithium film deposited using the four additives, while the other electrode was a commercially available lithium foil. Under a small current density such as $\sim 0.1 \text{ mA cm}^{-2}$, the cycle performance was relatively good (not shown here) using the solution with the four additives. However, the effect of the additives may be prominent under a large current density; therefore, we will study the cycle performance in detail in the near future.

4. Conclusions

The present study reports the combination of four additives for the production of a macroscopically uniform and flat lithium thin film by electrodeposition. The roles of the additives were studied by EQCM and XPS. The results suggest that each additive has its own role, and thus they should be used in combination. Although we have found that the four additives are effective for the production of macroscopically flat and smooth lithium film, it has not been clarified well whether they can be used as additives of a battery electrolyte. We are confident that the macroscopically uniform and flat lithium thin films produced in this study would be beneficial in designing metallic lithium-based batteries with a low cost.

CRedit authorship contribution statement

Kazuhiro Fukami: Conceptualization, Methodology, Validation, Supervision, Project administration, Funding acquisition, Writing – original draft. **Akihiro Sakurai:** Validation, Writing – review & editing. **Takamitsu Tsujimoto:** Validation, Writing – review & editing. **Masaki Yamagami:** Validation. **Atsushi Kitada:** Validation, Writing – review & editing, Funding acquisition. **Kota Morimoto:** Validation. **Kiho Nishioka:** Validation. **Shuji Nakanishi:** Conceptualization, Methodology, Validation, Writing – review & editing. **Yusuke Yoshikane:** Validation. **Toshimitsu Nagao:** Conceptualization, Methodology, Validation, Writing – review & editing. **Jun-ichi Katayama:** Conceptualization, Methodology, Validation, Writing – review & editing. **Kuniaki Murase:** Validation, Writing – review & editing, Funding acquisition.

Declaration of Competing Interest

The authors declare that they have no known competing financial interests or personal relationships that could have appeared to influence the work reported in this paper.

Acknowledgment

This work was supported by JSPS Grant-in-Aid for Scientific Research B (Grant Number 21H01670; K.F., and 19H02490; A.K.), Grant-in-Aid for Scientific Research S (Grant Number 20H05663; K.M.), and Grant-in-Aid for Challenging Research (Exploratory) (Grant Number 18K18941; K.M.).

References

- [1] R. Akolkar, Mathematical model of the dendritic growth during lithium electrodeposition, *J. Power Sources* 232 (2013) 23–28.
- [2] J.K. Stark, Y.i. Ding, P.A. Kohl, Nucleation of electrodeposited lithium metal: dendritic growth and the effect of co-deposited sodium, *J. Electrochem. Soc.* 160 (9) (2013) D337–D342.
- [3] J. Steiger, D. Kramer, R. Mönig, Mechanisms of dendritic growth investigated by in situ light microscopy during electrodeposition and dissolution of lithium, *J. Power Sources* 261 (2014) 112–119.
- [4] S.-K. Jeong, H.-Y. Seo, D.-H. Kim, H.-K. Han, J.-G. Kim, Y.B. Lee, Y. Iriyama, T. Abe, Z. Ogumi, Suppression of dendritic lithium formation by using concentrated electrolyte solutions, *Electrochem. Commun.* 10 (4) (2008) 635–638.
- [5] B. Wu, J. Lochala, T. Taverne, J. Xiao, The interplay between solid electrolyte interface (SEI) and dendritic lithium growth, *Nano Energy* 40 (2017) 34–41.
- [6] L. Li, S. Li, Y. Lu, Suppression of dendritic lithium growth in lithium metal-based batteries, *Chem. Commun.* 54 (50) (2018) 6648–6661.
- [7] Y. Liu, X. Xu, M. Sadd, O.O. Kapitanova, V.A. Krivchenko, J. Ban, J. Wang, X. Jiao, Z. Song, J. Song, S. Xiong, A. Matic, Insight into the critical role of exchange current density on electrodeposition behavior of lithium metal, *Adv. Sci.* 8 (2021) 1–11.
- [8] W. Dong, K. Wang, J. Han, Y. Yu, G. Liu, C. Li, P. Tong, W. Li, C. Yang, Z. Lu, Regulating lithium electrodeposition with laser-structured current collectors for stable lithium metal batteries, *ACS Appl. Mater. Interfaces* 13 (7) (2021) 8417–8425.
- [9] Z. Chen, W. Chen, H. Wang, C. Zhang, X. Qi, L. Qie, F. Wu, L. Wang, F. Yu, Lithiophilic anchor points enabling endogenous symbiotic Li_3N interface for homogeneous and stable lithium electrodeposition, *Nano Energy* 93 (2022), 106836.
- [10] Y. Liu, X. Xu, O.O. Kapitanova, P.V. Evdokimov, Z. Song, A. Matic, S. Xiong, Electro-chemo-mechanical modeling of artificial solid electrolyte interphase to enable uniform electrodeposition of lithium metal anodes, *Adv. Energy Mater.* 2103589 (2022) 2103589.
- [11] M. Schlesinger, M. Paunovic, *Modern Electroplating*, John Wiley & Sons Inc, NY, 2000.
- [12] S. Shiraishi, K. Kanamura, Z.-I. Takehara, Surface condition changes in lithium metal deposited in nonaqueous electrolyte containing HF by dissolution-deposition cycles, *J. Electrochem. Soc.* 146 (5) (1999) 1633–1639.
- [13] S. Shiraishi, K. Kanamura, Z.-I. Takehara, Study of the surface composition of highly smooth lithium deposited in various carbonate electrolytes containing HF, *Langmuir* 13 (13) (1997) 3542–3549.
- [14] Y.M. Lee, J.E. Seo, Y.-G. Lee, S.H. Lee, K.Y. Cho, J.-K. Park, Effects of triacetoxymethylsilane as SEI layer additive on electrochemical performance of lithium metal secondary battery, *Electrochem. Solid-State Lett.* 10 (9) (2007) A216, <https://doi.org/10.1149/1.2750439>.
- [15] D. Aurbach, Y. Gofer, M. Ben-Zion, P. Aped, The behaviour of lithium electrodes in propylene and ethylene carbonate: The major factors that influence Li cycling efficiency, *J. Electroanal. Chem.* 339 (1992) 451–471.
- [16] S. Matsuda, K. Nishioka, S. Nakanishi, High-throughput combinatorial screening of multi-component electrolyte additives to improve the performance of Li metal secondary batteries, *Sci. Rep.* 9 (2019) 1–3.
- [17] N. Serizawa, S. Seki, K. Takei, H. Miyashiro, K. Yoshida, K. Ueno, N. Tachikawa, K. Dokko, Y. Katayama, M. Watanabe, T. Miura, EQCM measurement of deposition and dissolution of lithium in glyme-Li salt molten complex, *J. Electrochem. Soc.* 160 (9) (2013) A1529–A1533.
- [18] E.A. Pavlatou, M. Raptakis, N. Spyrellis, Synergistic effect of 2-butyne-1,4-diol and pulse plating on the structure and properties of nickel nanocrystalline deposits, *Surf. Coatings Technol.* 201 (8) (2007) 4571–4577.
- [19] J.J. Yeh, I. Lindau, Atomic subshell photoionization cross sections and asymmetry parameters: $1 < Z < 103$, *At. Data Nucl. Data Tables.* 32 (1985) 1–155.
- [20] Y. Diao, K. Xie, S. Xiong, X. Hong, Analysis of polysulfide dissolved in electrolyte in discharge-charge process of Li-S battery, *J. Electrochem. Soc.* 159 (4) (2012) A421–A425.
- [21] M. Nojabaei, K. Küster, U. Starke, J. Popovic, J. Maier, Solid electrolyte interphase evolution on lithium metal in contact with glyme-based electrolytes, *Small* 16 (23) (2020) 2000756, <https://doi.org/10.1002/sml.v16.2310.1002/sml.202000756>.